

Phase transitions in antiferromagnetic quantum spin chains with bond alternation

Shoji Yamamoto

*Institute für Theoretische Physik, Universität Hannover, Appelstrasse 2, 30167 Hannover, Germany
and Department of Physics, Faculty of Science, Okayama University, Okayama 700, Japan**

(Received 3 September 1996)

We study the phase transitions in antiferromagnetic quantum spin chains with bond alternation, $\mathcal{H} = J \sum_i [1 - (-1)^i \delta] \mathbf{S}_i \cdot \mathbf{S}_{i+1}$, of spin $S = 1, 3/2$, and 2. On the one hand, using a transfer matrix technique, we make a simple variational approach, which results in the better estimates of the transition points than by the $O(3)$ nonlinear- σ -model quantum field theory. On the other hand, employing a quantum Monte Carlo method, we calculate the generalized string order parameter, $O_{\text{string}}^z(\theta) = \lim_{L \rightarrow \infty} O_{\text{string}}^z(\theta; L)$ with $O_{\text{string}}^z(\theta; L) = \langle S_{L/4}^z \prod_{j=L/4}^{3L/4-1} \exp[i\theta S_j^z] S_{3L/4}^z \rangle$. It turns out that the transition points are successfully detected by observing the overall behavior of $O_{\text{string}}^z(\theta)$ at various values of δ . Investigating the dependences of $O_{\text{string}}^z(\theta; L)$ on θ, L , and S , we discuss the applicability of the valence-bond-solid picture to the ground states of the present Hamiltonian. [S0163-1829(97)01406-9]

I. INTRODUCTION

The qualitative difference of the low temperature properties between integer-spin and half-odd-integer-spin one-dimensional Heisenberg antiferromagnets predicted by Haldane¹ is now widely accepted and may be one of common sense in the field of condensed matter physics. In fact various numerical methods made sure of both the existence of the excitation gap immediately above the ground state and the exponential decay of the ground-state spin correlation function not only in the $S=1$ case²⁻⁶ but also in the $S=2$ case.⁷⁻¹⁴

However, there are brand-new attempts¹⁵⁻¹⁹ to find out a more generic criterion for whether the system is massive or massless, where integer-spin and half-odd-integer-spin chains are not distinguished but are globally treated in a wider Hamiltonian space. Developing the $O(3)$ nonlinear- σ -model quantum field theory,¹ Affleck²⁰ already pointed out a few years after Haldane's conjecture that even integer-spin chains should be critical if a certain interaction is added to the pure Heisenberg Hamiltonian. His argument^{20,21} was unique in that he made such a suggestion not introducing an anisotropic term but breaking the symmetry of parity. In recent years, motivated by Affleck's prediction, several authors^{15-19,22-25} numerically investigated the Heisenberg Hamiltonian with bond alternation,

$$\mathcal{H} = J \sum_i [1 - (-1)^i \delta] \mathbf{S}_i \cdot \mathbf{S}_{i+1}, \quad (1.1)$$

where $\mathbf{S}_i^2 = S(S+1)$, which is expected to be in the massless phase when the so-called topological angle $\varphi \equiv 2\pi S(1-\delta)$ is equal to $\pi \pmod{2\pi}$,²⁰ namely, to encounter successive phase transitions of $2S$ times while δ moves from -1 to 1. Singh and Gelfand²² made the first approach to detect the critical point in the case of $S=1$ using a series-expansion method. Since then, density-matrix renormalization-group,²³ quantum Monte Carlo,^{16,24} and exact diagonalization²⁵ methods were in succession applied to the $S=1$ study and they all concluded that the critical point actually exists but is located

at $\delta = \delta_c \approx 0.25$ which somewhat deviates from the field-theoretical prediction, $\delta_c = 1/2$. Quite recently, the $S=3/2$ case¹⁸ was also discussed, making use of the numerical renormalization-group technique and the critical point was detected at $\delta = \delta_c \approx 0.42$, still showing a quantitative discrepancy from the field-theoretical prediction, $\delta_c = 2/3$. In the $S=2$ case, the transition points have not been specified yet, but three distinctive phases have been actually observed in the region $0 \leq \delta \leq 1$.¹⁹

Thus, it is quite likely that the phase transitions and the critical phenomena of the present (or possibly more extensive) Hamiltonians are described in terms of a generic scenario. In this context, it has been pointed^{18,19} out that the successive phase transitions may be, to a certain extent, regarded as ones between the so-called valence-bond-solid (VBS) states^{26,27} of different types, which are schematically shown in Fig. 1. On the other hand, the present author^{15,16} has shown that the critical points of the $S=1$ chain belong to the same universality class as the $S=1/2$ Heisenberg antiferromagnet. In such circumstances, it is unfortunate that in contrast to the vigorous argument in the $S=1$ case, there appeared few works in the larger-spin cases yet. Thus, assuming that the half-odd-integer- S Heisenberg points are all massless critical,^{1,28-30} here we treat the Hamiltonian (1.1) of $S=1, 3/2$, and 2. We adopt the periodic boundary condition and therefore treat the region $0 \leq \delta \leq 1$, because now the Hamiltonians with $\pm \delta$ should be equivalent to each other.

Calculation of the gap between the ground state and the first excited state may be the most naive and thus explicit approach in investigating the continuous phase transitions. However, the rapid decrease of the gap in magnitude with an increase of S clearly makes such an approach less feasible in the larger-spin cases. It is also unfortunate that the energy gap shows a slow convergence in taking the thermodynamic limit. For instance, in the $S=2$ case, the Haldane gap, that is, the gap at the Heisenberg point, is already smaller than $0.1J$ (Refs. 8-14) and is being discussed with chains of length larger than a few hundred sites.^{12,14} Therefore, even with the density-matrix renormalization-group method^{12,18} and the approved quantum Monte Carlo approach,^{13,14} it may

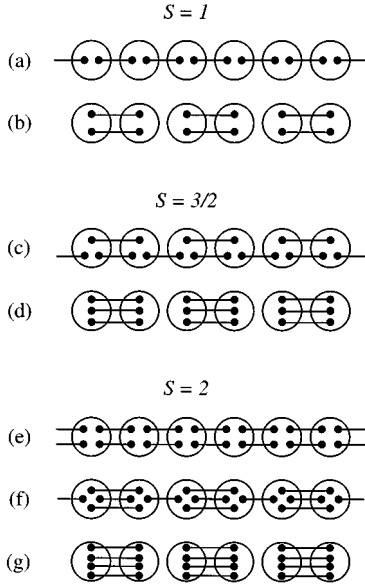


FIG. 1. Schematic representations of the VBS states for $S=1$ (a) and (b), $S=3/2$ (c) and (d), and $S=2$ (e)–(g), where the symbol \bullet and the segment denote a spin $1/2$ and a singlet pair, respectively, while the circle represents an operation of constructing a spin S by symmetrizing the $2S$ spin $1/2$'s inside. The configurations (a)–(g) are called $(1, 1)$, $(2, 0)$, $(2, 1)$, $(3, 0)$, $(2, 2)$, $(3, 1)$, $(4, 0)$ VBS states, respectively. We find out $2S+1$ states of this type in the spin- S case. Under the periodic boundary condition, all the rest are essentially identified with any of the present ones, because reversing the sign of δ is no more than interchanging the two sublattices. Thus, while the system goes through all the configurations, it encounters $2S$ transition points.

be rather hard to directly detect the massless points of the $S=2$ chain. Thus here we no longer persist in observing the energy gap itself but expect the generalized string order parameter²⁷

$$O_{\text{string}}^z(\theta) = \lim_{|i-j| \rightarrow \infty} \left\langle S_i^z \prod_{k=i}^{j-1} \exp[i\theta S_k^z] S_j^z \right\rangle, \quad (1.2)$$

to play an indicator of the phase transitions, where $\langle A \rangle$ denotes the grand-state average of the operator A . This idea is based on the fact that each of the VBS states has a unique θ dependence of $O_{\text{string}}^z(\theta)$.^{17,27} More specifically, under a certain applicability of the VBS picture to the present Hamiltonian, its ground states may be qualitatively identified with one of the VBS states and therefore the transition points between them should be successfully detected by observing $O_{\text{string}}^z(\theta)$ as a function of θ at various values of δ . Therefore we employ a quantum Monte Carlo method to calculate $O_{\text{string}}^z(\theta; L)$.

On the other hand, we would rather aim to reveal the physical mechanism of this phenomenon than totally devote ourselves to specification of the transition points. From this point of view, we discuss the subject in another way making use of simple variational wave functions which are linear combinations of the proper VBS states. Although the approach is so naive as to result in the discontinuous phase

transitions, it is more useful than the $O(3)$ nonlinear- σ -model quantum field theory in estimating the transition points.

This paper is organized as follows. In Sec. II, defining the appropriate transfer matrices,^{17,25,31,32} we obtain the individual forms of $O_{\text{string}}^z(\theta)$ which characterize the VBS states shown in Fig. 1. In Sec. III, we perform the variational calculation and qualitatively verify the underlying mechanism of the successive phase transitions. In Sec. IV, we present the quantum Monte Carlo study. After we briefly describe the numerical procedure, we estimate the transition points making the best use of $O_{\text{string}}^z(\theta)$. Section V is devoted to summary and discussion, where we graphically present all the results obtained and discuss the validity of the VBS picture for the ground states of the present Hamiltonian.

II. GENERALIZED STRING ORDER PARAMETER

Let us call the VBS state with m valence bonds between sites $2j-1$ and $2j$ and n between $2j$ and $2j+1$ the (m, n) VBS state. The usual Affleck-Kennedy-Lieb-Tasaki (AKLT) state²⁶ in the case of $S=m$ is identified with the (m, m) VBS state, which is invariant under translation. We show in Sec. III that within a simple variational approach, even the VBS states themselves play the approximate ground states of the present Hamiltonian with certain values of δ .

Using the Schwinger boson representation,

$$\begin{aligned} S_i^+ &= a_i^\dagger b_i, & S_i^z &= \frac{1}{2}(a_i^\dagger a_i - b_i^\dagger b_i), \\ S_i^- &= a_i b_i^\dagger, & \hat{S}_i &= \frac{1}{2}(a_i^\dagger a_i + b_i^\dagger b_i), \end{aligned} \quad (2.1)$$

the (m, n) VBS state is written as

$$\begin{aligned} |(m, n)\text{VBS}\rangle &= \prod_{j=1}^{L/2} (a_{2j-1}^\dagger b_{2j}^\dagger - b_{2j-1}^\dagger a_{2j}^\dagger)^m \\ &\quad \times (a_{2j}^\dagger b_{2j+1}^\dagger - b_{2j}^\dagger a_{2j+1}^\dagger)^n |0\rangle, \end{aligned} \quad (2.2)$$

where $|0\rangle$ is the Bose vacuum and L is the chain length. Due to the periodic boundary condition, we adopt the identities, $a_{L+1}^\dagger = a_1^\dagger$ and $b_{L+1}^\dagger = b_1^\dagger$. It is of great use to introduce an alternative representation of matrix-product type:

$$|(m, n)\text{VBS}\rangle = \text{Tr}[g_1^A \otimes g_2^B \otimes \cdots \otimes g_{L-1}^A \otimes g_L^B], \quad (2.3)$$

where at sites $2j-1$ and $2j$ we define the $n \times m$ and the $m \times n$ matrices, g_{2j-1}^A and g_{2j}^B respectively, as

$$\begin{aligned} g_{2j-1}^A(p; q) &= (-1)^{n-p} \sqrt{n C_{pm} C_q} (a_{2j-1}^\dagger)^{n-p+q} \\ &\quad \times (b_{2j-1}^\dagger)^{m+p-q} |0\rangle_{2j-1}, \end{aligned} \quad (2.4a)$$

$$\begin{aligned} g_{2j}^B(q; p) &= (-1)^{m-q} \sqrt{n C_{pm} C_q} (a_{2j}^\dagger)^{m+p-q} \\ &\quad \times (b_{2j}^\dagger)^{n-p+q} |0\rangle_{2j}, \end{aligned} \quad (2.4b)$$

with the local vacuum state $|0\rangle_i$. Here $g(r; s)$ denotes the (r, s) element of the matrix g . For the convenience of the later calculation, we list in the Appendix the concrete forms of the g matrices in terms of the S_i^z eigenstates.

In order to actually calculate the generalized string order parameter, we take the following expression:

$$O_{\text{string}}^z(\theta) = \lim_{L \rightarrow \infty} O_{\text{string}}^z(\theta; L), \quad (2.5)$$

where

$$O_{\text{string}}^z(\theta; L) = \left\langle S_{L/4}^z \prod_{j=L/4}^{3L/4-1} \exp[i\theta S_j^z] S_{3L/4}^z \right\rangle. \quad (2.6)$$

Defining the $n^2 \times m^2$ and the $m^2 \times n^2$ transfer matrices,

$$G^A(p, p'; q, q') = g_{2j-1}^{A\dagger}(p; q) g_{2j-1}^A(p'; q'), \quad (2.7a)$$

$$G^B(q, q'; p, p') = g_{2j}^{B\dagger}(q; p) g_{2j}^B(q'; p'), \quad (2.7b)$$

we can straightforwardly evaluate $O_{\text{string}}^z(\theta; L)$ for each VBS state as

$$O_{\text{string}}^z(\theta; L) = \frac{\text{Tr}[(G^A G^B)^{L/4-1} G^A P^B (Q^A Q^B)^{L/4-1} Q^A R^B]}{\text{Tr}[(G^A G^B)^{L/2}]}, \quad (2.8)$$

where

$$P^B(q, q'; p, p') = g_{2j}^{B\dagger}(q; p) S_{2j}^z \exp[i\theta S_{2j}^z] g_{2j}^B(q'; p'), \quad (2.9a)$$

$$Q^A(p, p'; q, q') = g_{2j-1}^{A\dagger}(p; q) \exp[i\theta S_{2j-1}^z] g_{2j-1}^A(p'; q'), \quad (2.9b)$$

$$Q^B(q, q'; p, p') = g_{2j}^{B\dagger}(q; p) \exp[i\theta S_{2j}^z] g_{2j}^B(q'; p'), \quad (2.9c)$$

$$R^B(q, q'; p, p') = g_{2j}^{B\dagger}(q; p) S_{2j}^z g_{2j}^B(q'; p'). \quad (2.9d)$$

It may be noted that as far as we take an interest only in the thermodynamic-limit properties, G^A and G^B should be efficiently reduced in their dimensions (into the $n \times m$ and the $m \times n$ matrices).¹⁷ Let us take a glance at a few examples of $O_{\text{string}}^z(\theta; L)$:

(a) $S = 1, m = n = 1$:

$$O_{\text{string}}^z(\theta; L) = \frac{[(4/9)(-3)^L + 4] \sin^2(\theta/2) + (8/3)(-3)^{(L/2)} \cos^2(\theta/2)}{(-3)^L + 3}, \quad (2.10)$$

(b) $S = 1, m = 2, n = 0$:

$$O_{\text{string}}^z(\theta; L) = \frac{4}{9} \sin^2 \theta, \quad (2.11)$$

(c) $S = 3/2, m = 2, n = 1$:

$$O_{\text{string}}^z(\theta; L) = \frac{6^{(L/2)} (25/36) \sin^2 \theta + 6^{(L/4)} (5/6) \cos \theta (4 \cos \theta + 1) + 4 \sin \theta \cos \theta}{6^{(L/2)} + 3}, \quad (2.12)$$

(d) $S = 3/2, m = 3, n = 0$:

$$O_{\text{string}}^z(\theta; L) = \frac{1}{4} \left[\frac{3}{2} \sin\left(\frac{3\theta}{2}\right) + \frac{1}{2} \sin\left(\frac{\theta}{2}\right) \right]^2. \quad (2.13)$$

Instead of carrying out further demonstration, we note that $O_{\text{string}}^z(\theta; L)$ generally shows an L dependence in the AKLT and the partially dimerized VBS states, while it is always free from L in the totally dimerized VBS states. Now, taking the $L \rightarrow \infty$ limit for $O_{\text{string}}^z(\theta; L)$, we obtain the characteristic θ dependences of the generalized string order parameter for each VBS state as follows:

(a) $S = 1, m = n = 1$:

$$O_{\text{string}}^z(\theta) = \frac{16}{9} \left[\frac{1}{2} \sin\left(\frac{\theta}{2}\right) \right]^2, \quad (2.14)$$

(b) $S = 1, m = 2, n = 0$:

$$O_{\text{string}}^z(\theta) = \frac{4}{9} \sin^2 \theta, \quad (2.15)$$

(c) $S = 3/2, m = 2, n = 1$:

$$O_{\text{string}}^z(\theta) = \frac{25}{36} \sin^2 \theta, \quad (2.16)$$

(d) $S = 3/2, m = 3, n = 0$:

$$O_{\text{string}}^z(\theta) = \frac{1}{4} \left[\frac{3}{2} \sin\left(\frac{3\theta}{2}\right) + \frac{1}{2} \sin\left(\frac{\theta}{2}\right) \right]^2, \quad (2.17)$$

(e) $S = 2, m = 2, n = 2$:

$$O_{\text{string}}^z(\theta) = \sin^2 \theta, \quad (2.18)$$

(f) $S = 2, m = 3, n = 1$:

$$O_{\text{string}}^z(\theta) = \frac{9}{25} \left[\frac{3}{2} \sin\left(\frac{3\theta}{2}\right) + \frac{1}{2} \sin\left(\frac{\theta}{2}\right) \right]^2, \quad (2.19)$$

(g) $S=2, m=4, n=0$:

$$O_{\text{string}}^z(\theta) = \frac{4}{25} [2\sin(2\theta) + \sin\theta]^2. \quad (2.20)$$

Finally in this section, we add that although $O_{\text{string}}^z(\theta; L)$ for the (m, n) VBS state becomes more and more complicated with the increase of m and n , the corresponding $O_{\text{string}}^z(\theta)$ is compactly written as²⁷

$$O_{\text{string}}^z(\theta) = |f_{m,n}(e^{i\theta})|^2, \quad (2.21)$$

where

$$f_{m,n}(z) = \frac{m+n+2}{2(m+2)(m+1)} \sum_{k=0}^m (2k-m)z^k. \quad (2.22)$$

III. VARIATIONAL APPROACH

The linear combination of all the possible $(m, 2S-m)$ VBS states may be a naive but suggestive variational wave function for the ground state of the present Hamiltonian of spin S . Such a trial wave function is reasonable to the extent that it is obviously singlet and includes the exact solutions at $\delta = \pm 1$, namely, the totally dimerized VBS states, in itself. The variational approach of this type²⁵ was actually made to the $S=1$ bilinear-biquadratic Hamiltonian with bond alternation and resulted in the qualitatively reliable ground-state phase diagram. Here we develop the argument to the larger-spin chains reviewing the $S=1$ case for the sake of reference. It is enough for us to treat only the $(m, 2S-m)$ VBS states with $m \geq S$ due to the equivalence of the $\delta < 0$ region to the $\delta > 0$ one under the periodic boundary condition.

A. $S=1$

The trial wave function for the region $0 \leq \delta \leq 1$ should be constructed from the AKLT and the totally dimerized VBS states as

$$|\Psi(\theta)\rangle = \cos\theta \frac{|(1,1)\text{VBS}\rangle}{\|(1,1)\text{VBS}\|} + \sin\theta \frac{|(2,0)\text{VBS}\rangle}{\|(2,0)\text{VBS}\|}, \quad (3.1)$$

where $\|A\|$ denotes the norm of the state vector $|A\rangle$. $|\Psi(\theta)\rangle$ is correctly normalized in the thermodynamic limit because of the asymptotic orthogonality,

$$\frac{\langle(2,0)\text{VBS}|(1,1)\text{VBS}\rangle}{\|(2,0)\text{VBS}\|\|(1,1)\text{VBS}\|} = \frac{2(-3)^{(L/2)}}{3^{L/4}\sqrt{3^L+3}(-1)^L} \rightarrow 0 (L \rightarrow \infty). \quad (3.2)$$

We further note that the orthogonality of this type still holds in the larger-spin cases,²⁷ namely, the matrix elements between the (m, n) VBS and the (m', n') VBS states necessarily vanish in the thermodynamic limit unless $m=m'$ and $n=n'$. With the compact expression (2.3) and the G matrices (2.7), it is straightforward to derive

$$\frac{\langle(1,1)\text{VBS}|\mathcal{H}|(1,1)\text{VBS}\rangle}{\|(1,1)\text{VBS}\|^2} = -\frac{4L[3^L+9(-1)^{L-2}]}{3[3^L+3(-1)^L]}, \quad (3.3a)$$

$$\frac{\langle(2,0)\text{VBS}|\mathcal{H}|(2,0)\text{VBS}\rangle}{\|(2,0)\text{VBS}\|^2} = -L(1+\delta), \quad (3.3b)$$

$$\frac{\langle(2,0)\text{VBS}|\mathcal{H}|(1,1)\text{VBS}\rangle}{\|(2,0)\text{VBS}\|\|(1,1)\text{VBS}\|} = -\frac{2}{3}L \left(-\frac{1}{\sqrt{3}}\right)^{L/2} (5+\delta). \quad (3.3c)$$

Here we certainly find that the matrix element (3.3c) vanishes in the $L \rightarrow \infty$ limit. Now we obtain

$$\lim_{L \rightarrow \infty} \frac{\langle\Psi(\theta)|\mathcal{H}|\Psi(\theta)\rangle}{L} = \left(\delta - \frac{1}{3}\right) \cos^2\theta - (1+\delta), \quad (3.4)$$

which leads to the simple solution,

$$\theta = 0 \quad \left(0 \leq \delta < \frac{1}{3}\right), \quad \theta = \frac{\pi}{2} \quad \left(\frac{1}{3} < \delta \leq 1\right). \quad (3.5)$$

Therefore, the variational ground state is the AKLT state itself for $|\delta| < 1/3$, while the totally dimerized VBS state itself for $|\delta| > 1/3$.

In the $S=1$ case, using various numerical methods, many authors²²⁻²⁵ have already come to an agreement with the conclusion $\delta_c \approx 0.25$. Therefore, the thus-obtained estimate of the transition point, $\delta_c = 1/3$, is much better than the field-theory result, $\delta_c = 1/2$. However, owing to the asymptotic orthogonality (3.2), the present variational calculation results in the discontinuous transition. In order to describe the real picture, that is, the continuous transition,^{15,16,20-25} in this context we may have to take the valence bonds beyond the nearest sites into the trial wave function.

B. $S=3/2$

The similar treatment is available in the $S=3/2$ case as well constructing the trial wave function as

$$|\Psi(\theta)\rangle = \cos\theta \frac{|(2,1)\text{VBS}\rangle}{\|(2,1)\text{VBS}\|} + \sin\theta \frac{|(3,0)\text{VBS}\rangle}{\|(3,0)\text{VBS}\|}. \quad (3.6)$$

The asymptotic orthogonality

$$\frac{\langle(3,0)\text{VBS}|(2,1)\text{VBS}\rangle}{\|(3,0)\text{VBS}\|\|(2,1)\text{VBS}\|} = \frac{2(-6)^{(L/2)}}{4^{L/2}\sqrt{6^{L/2}+3}} \rightarrow 0 \quad (L \rightarrow \infty), \quad (3.7)$$

again simplifies the calculation and we finally obtain

$$\lim_{L \rightarrow \infty} \frac{\langle\Psi(\theta)|\mathcal{H}|\Psi(\theta)\rangle}{L} = \frac{65}{48} \left(\delta - \frac{7}{13}\right) \cos^2\theta - \frac{15}{8}(1+\delta). \quad (3.8)$$

Therefore we reach the simple scenario just the same,

$$\theta = 0 \quad \left(0 \leq \delta < \frac{7}{13}\right), \quad \theta = \frac{\pi}{2} \quad \left(\frac{7}{13} < \delta \leq 1\right). \quad (3.9)$$

The recent density-matrix renormalization-group approach has concluded that $\delta_c \approx 0.42$, which is in good agreement with the present quantum Monte Carlo calculation which is shown in Sec. IV. Thus, as far as an estimation of the transition points is concerned, the simplest variational approach is still better than the semiclassical-limit field-theory result, $\delta_c = 2/3$.

C. $S=2$

The $S=2$ case can be discussed in the same way but the trial wave function is now constructed from the VBS states of three types as

$$|\Psi(\theta, \phi)\rangle = \cos\theta \frac{|(2,2)\text{VBS}\rangle}{\|(2,2)\text{VBS}\|} + \sin\theta \cos\phi \frac{|(3,1)\text{VBS}\rangle}{\|(3,1)\text{VBS}\|} + \sin\theta \sin\phi \frac{|(4,0)\text{VBS}\rangle}{\|(4,0)\text{VBS}\|}. \quad (3.10)$$

Making the full use¹⁷ of the asymptotic orthogonality, we obtain

$$\lim_{L \rightarrow \infty} \frac{\langle \Psi(\theta) | \mathcal{H} | \Psi(\theta) \rangle}{L} = \left[\frac{9}{5} \left(\delta - \frac{2}{3} \right) \cos^2 \phi + 3 \left(\frac{1}{2} - \delta \right) \right] \sin^2 \theta - \frac{9}{2}. \quad (3.11)$$

Therefore the variational ground state is given by

$$\begin{aligned} \theta=0, \quad \phi=0 & \quad \left(0 \leq \delta < \frac{1}{4} \right), \\ \theta=\frac{\pi}{2}, \quad \phi=0 & \quad \left(\frac{1}{4} < \delta < \frac{2}{3} \right), \\ \theta=\frac{\pi}{2}, \quad \phi=\frac{\pi}{2} & \quad \left(\frac{2}{3} < \delta \leq 1 \right). \end{aligned} \quad (3.12)$$

The quantum Monte Carlo calculation presented in Sec. IV shows that the second transition point (with the larger value of δ) is still better specified by the present approach than by the field theory. On the other hand, the two approximate treatments result in the same estimate of the first transition point (with the smaller value of δ), which implies that the ground states of the present Hamiltonian in the Haldane phase are less described in terms of the AKLT state for larger S . All the values obtained in this section are graphically presented in Sec. V together with the quantum Monte Carlo results and the field-theoretical prediction.

IV. QUANTUM MONTE CARLO APPROACH

It is well known that the AKLT states generally give considerably small correlation lengths³³ in comparison with ones on the Heisenberg points. Several authors^{34–36} have pointed out that once the Hamiltonian deviates from the AKLT point, there occur certain quantum fluctuations to break the perfect hidden order.³⁷ Thus the ground states of the present Hamiltonian should more or less deviate from the pure VBS configurations unless $|\delta|=1$. We have nonetheless found out in the preceding section that within the naivest variational treatment, all the possible $(m, 2S-m)$ VBS states play, in turn, the ground state of the present Hamiltonian of spin S while δ moves from -1 to 1 . The result allows us to expect that the VBS picture is still valid with the present Hamiltonian. The overall behavior of $O_{\text{string}}^z(\theta)$ actually supports the quali-

tative applicability of the VBS scenario to the successive phase transitions.

A. Numerical procedure

Here $O_{\text{string}}^z(\theta; L)$ is evaluated as the canonical average of $\hat{O}_{\text{string}}^z(\theta; L) = S_{L/4}^z \prod_{j=L/4}^{3L/4-1} \exp[i\theta S_j^z] S_{3L/4}^z$ at a sufficiently low temperature $\beta^{-1} = k_B T$:

$$O_{\text{string}}^z(\theta; L) = \frac{\text{Tr}[e^{-\beta \mathcal{H}} \hat{O}_{\text{string}}^z(\theta; L)]}{\text{Tr}[e^{-\beta \mathcal{H}}]}. \quad (4.1)$$

Decomposing the partition function $Z \equiv \text{Tr}[e^{-\beta \mathcal{H}}]$ as

$$Z \simeq \text{Tr} \left[\left(\prod_{i=1,3,\dots} e^{-\beta h_{i,i+1}/n} \prod_{i=2,4,\dots} e^{-\beta h_{i,i+1}/n} \right)^n \right], \quad (4.2)$$

with a Trotter number n and local Hamiltonians

$$h_{i,i+1} = J[1 - (-1)^i \delta] \mathbf{S}_i \cdot \mathbf{S}_{i+1}, \quad (4.3)$$

we carry out the world-line Monte Carlo sampling³⁸ on the equivalent $(1+1)$ -dimensional Ising system³⁹ of $L \times 2n$ size. We take a set of values for n and the n dependence is extrapolated into the $n \rightarrow \infty$ limit. Since the finite n effect on $O_{\text{string}}^z(\theta)$ is remarkably variable according to θ , the $n \rightarrow \infty$ extrapolation is essential in observing the overall behavior of $O_{\text{string}}^z(\theta)$. The numerical algorithm to update the spin configuration is detailed elsewhere,⁴⁰ which should be well designed especially for large-spin systems of great degrees of freedom so as to obtain reliable estimates within feasible Monte Carlo steps.

We treated the chains of $L=16, 32$, and 64 in the $S=1$ case, while in the larger-spin cases we calculated the chains of length up to $L=128$. We took $k_B T/J=0.02$ in combination with $n=40, 60, 80$, and 120 . Preliminary calculations at $k_B T/J=0.04$ and 0.02 resulted in almost the same estimates within the numerical accuracy and thus the temperature $k_B T/J=0.02$ is reliable enough to describe the ground-state properties. We calculated $O_{\text{string}}^z(\theta)$ setting θ to a finite set (generally 17 sometimes 33) of evenly spaced values between 0 and π and the θ dependence is interpolated for the sake of presentation. The numerical precision in the final results is almost down to two decimal places, namely, there may be, at most, slight uncertainty in the second decimal place. The largest uncertainty appears in the vicinity of the critical points. The dominant errors occur generally in the Monte Carlo sampling itself rather than in the $n \rightarrow \infty$ or the $L \rightarrow \infty$ extrapolation.

B. $S=1$

In Fig. 2 we show $O_{\text{string}}^z(\theta)$ as a function of θ changing the value of δ . It is obvious that with an increase of δ the system encounters the phase transition between the Haldane and the dimer phases which are qualitatively identified with the $(1,1)$ VBS and the $(2,0)$ VBS states, respectively. While the system already looks completely dimerized at $\delta=0.5$, the

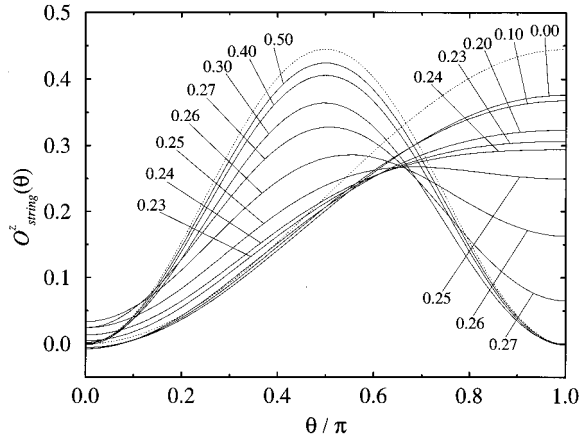


FIG. 2. Generalized string order parameter $O_{\text{string}}^z(\theta)$ as a function of θ at various values of δ in the $S=1$ case. The dashed lines represent ones for the AKLT [Fig. 1(a)] and the (2,0) VBS [Fig. 1(b)] states, namely, Eqs. (2.14) and (2.15).

ground state at $\delta=0.0$ still deviates from the AKLT configuration to a certain extent. The reduction of the order parameter at $\theta=\pi$ is nothing but a consequence of the domain walls in the hidden order.³⁵ However, interestingly, the qualitative θ dependence is kept almost unbroken on both sides of the transition point. If we specify the phase transition through a change of the θ dependence in the vicinity of $\theta=\pi$, that is, the change from the convex curve to the concave one, we come to the conclusion that $\delta_c \approx 0.245$, which is in good agreement with the well-accepted estimate $\delta_c \approx 0.25$ (Refs. 22–25) obtained with various methods and from various standpoints.

It is interesting to observe the size dependences of $O_{\text{string}}^z(\theta; L)$ in considering the applicability of the VBS picture to the present Hamiltonian. Let us recall Eqs. (2.10) and (2.11), namely, that $O_{\text{string}}^z(\theta; L)$ shows an actual size dependence in the AKLT state, while no size dependence in the totally dimerized VBS state. We show in Fig. 3 the size dependences of $O_{\text{string}}^z(\theta; L)$ at $\delta=0.0$ [Fig. 3(a)] and $\delta=0.5$ [Fig. 3(b)], which are typical of the Haldane and the dimer phases, respectively. We find that the Haldane phase gives a much more significant size dependence than the dimer phase, which is qualitatively consistent with the VBS scenario. However, the size dependence of Eq. (2.10) is so weak as to exhibit no visible difference in the scale of Fig. 3(a). Therefore, as for the short-chain properties, there should be remarkable differences between the present and the AKLT models. This may be attributed to the discrepancy of the (Néel) correlation length ξ . Although even the pure Heisenberg Hamiltonian gives $\xi \approx 6$,^{3–6} the AKLT model shows the extremely short-range correlation, $\xi = 1/\ln 3$. It is well understood that $O_{\text{string}}^z(\theta=0; L)$, that is, the Néel correlation looks significant unless $L \gg \xi$ in Fig. 3(a).

C. $S=3/2$

Figure 4 shows $O_{\text{string}}^z(\theta)$ as a function of θ at various values of δ . We find the transition between the intermediate and the dimer phases which are qualitatively identified with the (2,1) VBS and the (3,0) VBS states, respectively. The

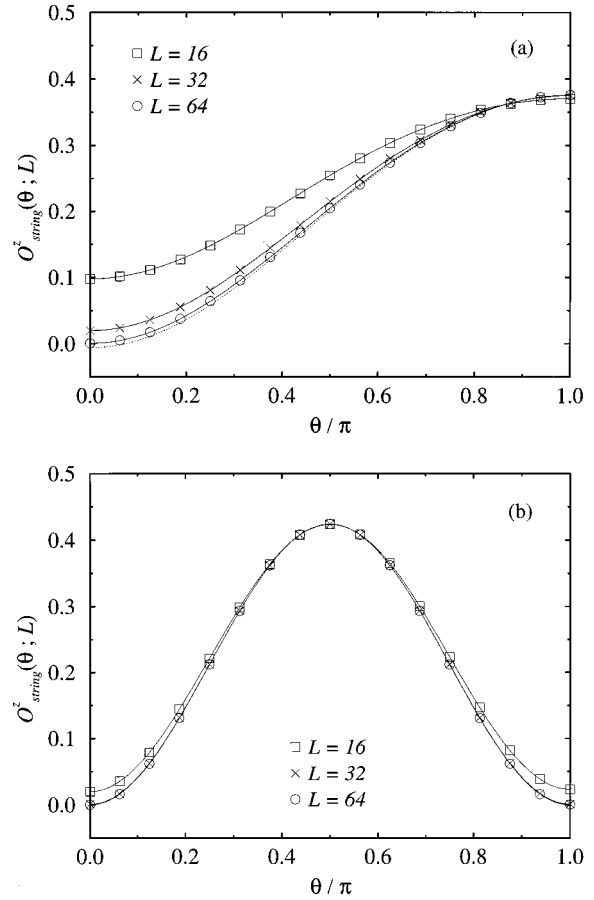


FIG. 3. Size dependence of $O_{\text{string}}^z(\theta; L)$ as a function of θ at $\delta=0.0$ (a) and $\delta=0.5$ (b), where the ground state is qualitatively described by the AKLT [Fig. 1(a)] and the (2,0) VBS [Fig. 1(b)] states, respectively. Here the dashed line represents the $L \rightarrow \infty$ behavior, namely, the corresponding $O_{\text{string}}^z(\theta)$, obtained by extrapolating the raw data.

overall behavior of $O_{\text{string}}^z(\theta)$ well supports the applicability of the VBS picture. However, it seems that the maximum-value position of $O_{\text{string}}^z(\theta)$ in the intermediate phase slightly deviates from $\theta=\pi/2$ given by the pure (2,1) VBS state. Carefully observing the θ dependences around $\theta=\pi$ again, we conclude that $\delta_c = 0.43 \pm 0.01$, which coincides with the recent pioneering estimate $\delta_c = 0.42 \pm 0.02$ (Ref. 18) within the numerical accuracy. Now the generalized string order parameter may be really recognized as a reliable indicator of the phase transitions.

Let us observe size dependences of $O_{\text{string}}^z(\theta; L)$. We show in Fig. 5 the size dependences of $O_{\text{string}}^z(\theta; L)$ at $\delta=0.2$ [Fig. 5(a)] and $\delta=0.6$ [Fig. 5(b)], which are typical of the intermediate and the dimer phases, respectively. It is clear that the finite size effect is much more strong in the intermediate phase than in the dimer phase, which is qualitatively consistent with Eqs. (2.12) and (2.13). However, the L dependence of Eq. (2.12) is much weaker than the one in Fig. 5(a). This quantitative difference is again due to the remarkable discrepancy of the correlation length. While the correlation length of the present model with $\delta=0.20$ is measured as $\xi \approx 10$, the (2,1) VBS state gives $\xi = 2/\ln 6$. We actually observe in Fig. 5(a) that the Néel correlation of the $L=32$ chain is still far from the bulk behavior.

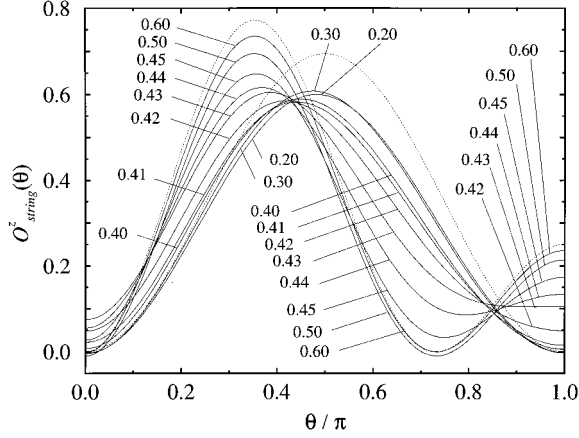


FIG. 4. Generalized string order parameter $O_{\text{string}}^z(\theta)$ as a function of θ at various values of δ in the $S=3/2$ case. The dashed lines represent ones for the (2,1) VBS [Fig. 1(c)] and the (3,0) VBS [Fig. 1(d)] states, namely, Eqs. (2.16) and (2.17).

D. $S=2$

Here the Haldane, the intermediate, and the dimer phases are expected to appear one by one, which are qualitatively identified with the (2,2) VBS, the (3,1) VBS, and the (4,0) VBS states, respectively. In Fig. 6 we show $O_{\text{string}}^z(\theta)$ as a function of θ changing the value of δ . Figures 6(a) and 6(b) focus on the first (Haldane-intermediate) and the second (intermediate-dimer) transitions, respectively. The θ dependences of $O_{\text{string}}^z(\theta)$ in the intermediate and the dimer phases still look consistent with ones of the (2,1) VBS and the (3,0) VBS states, respectively, whereas the (2,2) VBS state seems to describe less the Haldane phase of the present Hamiltonian. Even at $\delta=0.0$, the maximum-value position of $O_{\text{string}}^z(\theta)$ clearly deviates from $\pi/2$ given by the AKLT state. This is a contrast to the $S=1$ case. However, the overall behavior of $O_{\text{string}}^z(\theta)$ still bears a certain analogy to the VBS picture to the extent that it enables us to detect the transition points. The θ dependences in the vicinity of $\theta=\pi$ remain useful and we conclude that $\delta_{c1}=0.18\pm 0.01$ and $\delta_{c2}=0.545\pm 0.005$ for the first and the second transitions, respectively. The second transition seems to take place more sharply and therefore it is better specified than the first one.

We show in Fig. 7 how $O_{\text{string}}^z(\theta;L)$ converges into $O_{\text{string}}^z(\theta)$ at $\delta=0.0$ [Fig. 7(a)], 0.4 [Fig. 7(b)], and 0.7 [Fig. 7(c)], where the system is in the Haldane, the intermediate, and the dimer phases, respectively. It is Figs. 7(a) and 7(b) that show significant size dependences, which are rather strong around the minimum-value points, while relatively weak around the maximum-value points. In general, with decrease of L , the maximum-value points move left and the curves become flatter in the vicinity of $\theta=0$ and π . This behavior somewhat resembles one observed in Fig. 6 with increase of δ and thus implies that for small L 's the system with its small gap and large correlation length still looks critical.¹³

V. SUMMARY AND DISCUSSION

We have extensively investigated the successive phase transitions of the antiferromagnetic Heisenberg chains with

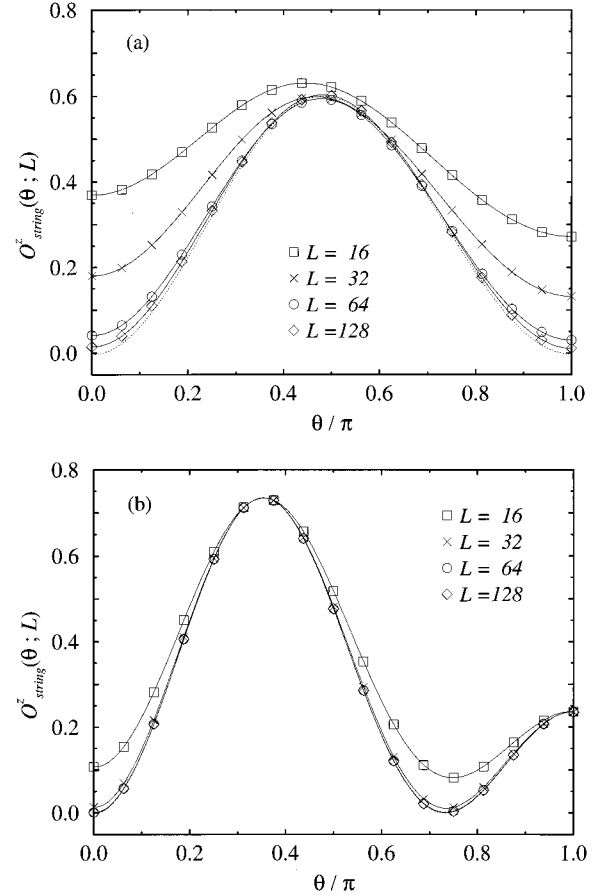


FIG. 5. Size dependence of $O_{\text{string}}^z(\theta;L)$ as a function of θ at $\delta=0.2$ (a) and $\delta=0.6$ (b), where the ground state is qualitatively described by the (2,1) VBS [Fig. 1(c)] and the (3,0) VBS [Fig. 1(d)] states, respectively. Here the dashed line represents the $L\rightarrow\infty$ behavior, namely, the corresponding $O_{\text{string}}^z(\theta)$, obtained by extrapolating the raw data.

bond alternation being based on the applicability of the VBS picture to this phenomenon. For the purpose of understanding the nature of each phase, in Table I we characterize the (m,n) VBS state by the Néel order parameter $O_{\text{Néel}}\equiv O_{\text{string}}^z(0)$ and den Nijs–Rommelse string order parameter $O_{\text{NR}}\equiv O_{\text{string}}^z(\pi)$. Here \circ and \times represent surviving and vanishing order parameters, respectively. Since O_{NR} is directly related with the hidden $Z_2\times Z_2$ symmetry^{27,41} for integer spins, we indicate as well whether it is broken or not in the cases of $S=1$ and 2. The quantum Monte Carlo calculation has shown that the phase transitions in the present model are almost consistent with this VBS picture.

The transition points have been estimated not only employing the quantum Monte Carlo method but also with use of the simple variational wave functions. The quantum Monte Carlo results well coincide with all the previous estimates obtained through various approaches and therefore the generalized string order parameter does work as an indicator of the present successive phase transitions. It is useful to graphically present in Fig. 8 all the findings in comparison with the field-theoretical prediction.²⁰ All in all, the variational approach is better than the field-theoretical one. However, its quantitative superiority seems to be reduced with increase of S . This may be attributed to two reasons. On the

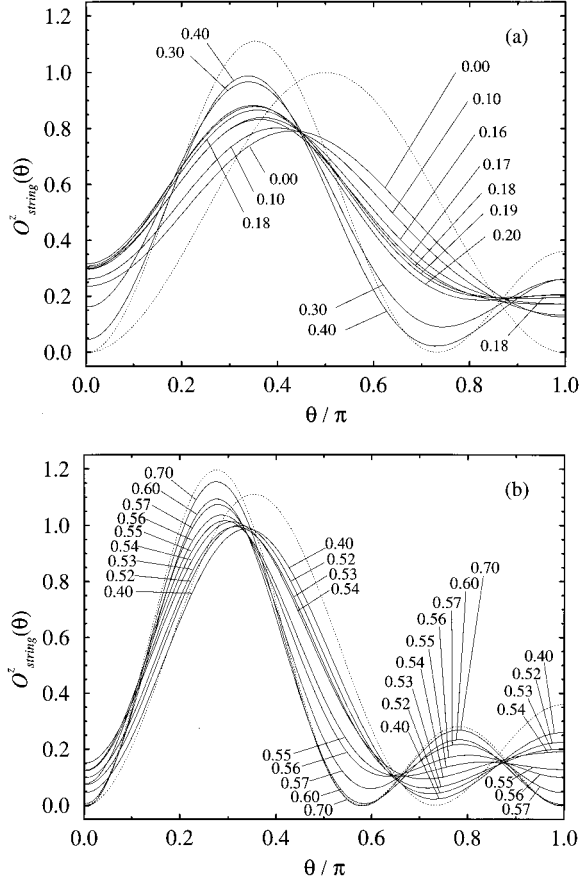


FIG. 6. Generalized string order parameter $O_{\text{string}}^z(\theta)$ as a function of θ at various values of δ in the $S=2$ case. The dashed lines represent ones for the AKLT [Fig. 1(e)], the (3,1) VBS [Fig. 1(f)] and the (4,0) VBS [Fig. 1(g)] states, namely, Eqs. (2.18), (2.19), and (2.20).

one hand, it is a matter of course that the $O(3)$ nonlinear- σ -model quantum field theory is more justified for larger S because of its semiclassical treatment. On the other hand, the present variational approach, which simply approximates each phase by one of the VBS states, is expected to become less valid with increase of S . In this context, let us take a look at the explicit expression of the spin- S Hamiltonian whose ground state is the (m, n) VBS state ($m+n=2S$). Such a Hamiltonian is easily constructed as^{17,26}

$$\mathcal{H}_{(m,n)\text{VBS}} = \sum_{i=1,3,\dots} P_n^S(\mathbf{S}_i \cdot \mathbf{S}_{i+1}) + \sum_{i=2,4,\dots} P_m^S(\mathbf{S}_i \cdot \mathbf{S}_{i+1}), \quad (5.1)$$

where

$$P_l^S(\mathbf{S}_i \cdot \mathbf{S}_{i+1}) = \frac{1}{N_l^S} \prod_{J=0}^l [2\mathbf{S}_i \cdot \mathbf{S}_{i+1} + 2S(S+1) - J(J+1)], \quad (5.2)$$

is the $(l+1)$ th-order polynomials of the exchange interaction $\mathbf{S}_i \cdot \mathbf{S}_{i+1}$ so as to project out the subspaces with $(\mathbf{S}_i + \mathbf{S}_{i+1})^2 > l(l+1)$; $l=0, 1, \dots, 2S$. Here N_l^S has been just introduced so as to take the coefficient of the linear term

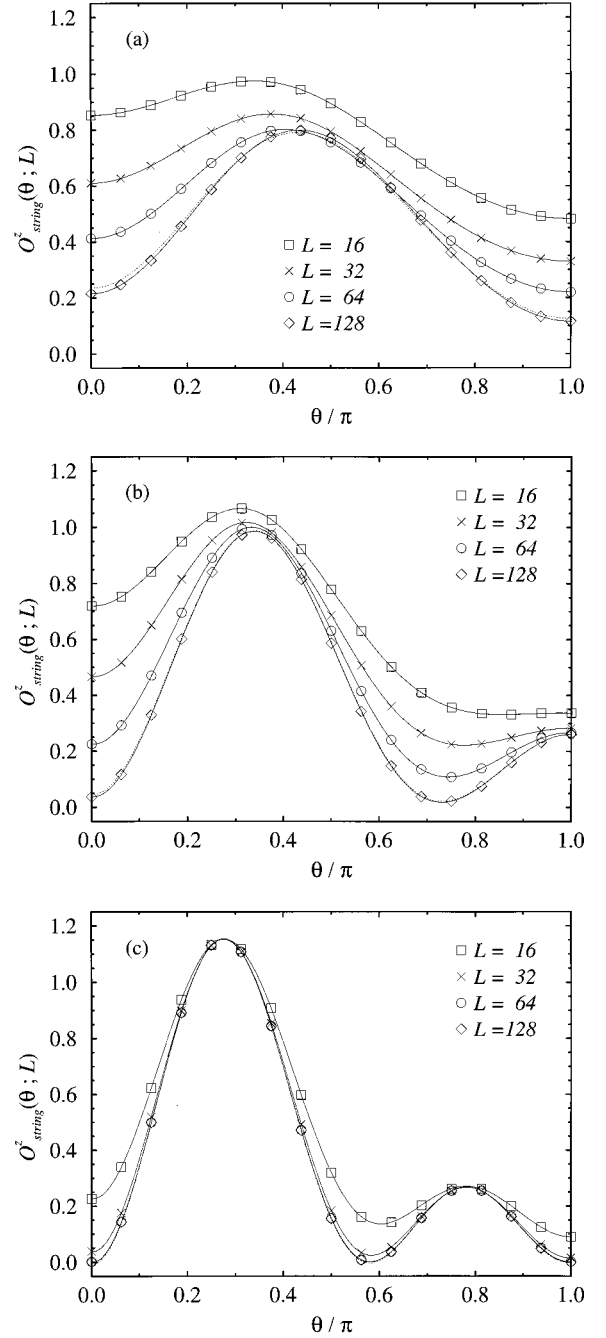


FIG. 7. Size dependence of $O_{\text{string}}^z(\theta; L)$ as a function of θ at $\delta=0.0$ (a), $\delta=0.4$ (b), and $\delta=0.7$ (c), where the ground state is qualitatively described by the AKLT [Fig. 1(e)], the (3,1) VBS [Fig. 1(f)], and the (4,0) VBS [Fig. 1(g)] states, respectively. Here the dashed line represents the $L \rightarrow \infty$ behavior, namely, the corresponding $O_{\text{string}}^z(\theta)$, obtained by extrapolating the raw data.

as unity. Since it is obvious that $P_{2S}^S(\mathbf{S}_i \cdot \mathbf{S}_{i+1})=0$, we write down in the following a few examples of $\mathcal{H}_{(m,n)\text{VBS}}$ with $m < 2S$:

$$\mathcal{H}_{(1,1)\text{VBS}} = \sum_{i=1}^L \left[\mathbf{S}_i \cdot \mathbf{S}_{i+1} + \frac{1}{3} (\mathbf{S}_i \cdot \mathbf{S}_{i+1})^2 + \frac{2}{3} \right], \quad (5.3)$$

$$\mathcal{H}_{(2,1)\text{VBS}} = \sum_{i=1}^L \left[\mathbf{S}_i \cdot \mathbf{S}_{i+1} + \frac{997 + (-1)^i 511}{3159} (\mathbf{S}_i \cdot \mathbf{S}_{i+1})^2 \right]$$

TABLE I. Nature of the (m, n) VBS state.

S	(m, n)	$O_{\text{Néel}}$	O_{NR}	$Z_2 \times Z_2$ symmetry
1	(1,1)	×	○	Broken
	(2,0)	×	×	Unbroken
	(2,1)	×	×	—
3/2	(3,0)	×	○	—
	(2,2)	×	×	Unbroken
2	(3,1)	×	○	Broken
	(4,0)	×	×	Unbroken

$$+ \frac{8\{1 + (-1)^i\}}{243} (\mathbf{S}_i \cdot \mathbf{S}_{i+1})^3 + \frac{5885}{5616}], \quad (5.4)$$

$$\mathcal{H}_{(2,2)\text{VBS}} = \sum_{i=1}^L \left[\mathbf{S}_i \cdot \mathbf{S}_{i+1} + \frac{2}{9} (\mathbf{S}_i \cdot \mathbf{S}_{i+1})^2 + \frac{1}{63} (\mathbf{S}_i \cdot \mathbf{S}_{i+1})^3 + \frac{10}{7} \right], \quad (5.5)$$

$$\mathcal{H}_{(3,1)\text{VBS}} = \sum_{i=1}^L \left[\mathbf{S}_i \cdot \mathbf{S}_{i+1} + \frac{87 + (-1)^i 67}{220} (\mathbf{S}_i \cdot \mathbf{S}_{i+1})^2 + \frac{7\{1 + (-1)^i\}}{90} (\mathbf{S}_i \cdot \mathbf{S}_{i+1})^3 + \frac{1 + (-1)^i}{180} (\mathbf{S}_i \cdot \mathbf{S}_{i+1})^4 + \frac{15}{11} \right]. \quad (5.6)$$

Thus, with an increase of S , the additional higher-order terms appear in the VBS Hamiltonians. We have actually observed in Figs. 2 and 6(a) that the ground state of the present Hamiltonian in the Haldane-phase region more and more deviates from the AKLT state as S increases. We have at the same time found in Figs. 4 and 6 that in the intermediate-phase region, the discrepancy between the ground state of the present Hamiltonian and the corresponding VBS state still looks less significant. This may be understood assuming that the interactions between the sites with stronger bonds, namely, between sites $2j-1$ and $2j$ here, are more effective than the rest, which is obvious in the strong-dimerization limit. In this sense, the VBS Hamiltonians $\mathcal{H}_{(m,n)\text{VBS}}$ with $n \leq 1$ or $m \leq 1$, which effectively stay within the second-order polynomials of the exchange interaction, are generally expected to qualitatively well describe the ground states of the present Hamiltonian. In other words, the smaller S and stronger dimerization, the better is the VBS picture applicable to the ground states of the present Hamiltonian.

Here we have concentrated ourselves on detecting a series of the transition points and revealing the underlying scenario. One of the following subjects to be discussed should be the universal character of the critical points. It is all the more interesting under the field-theoretical prediction^{29,30} of the generic critical behavior for a certain class of isotropic antiferromagnets. In fact several authors have already concluded that not only the $S=3/2$ Heisenberg point^{3,42,43} but also the present $S=1$ critical points^{15,16,25} belong to the same univer-

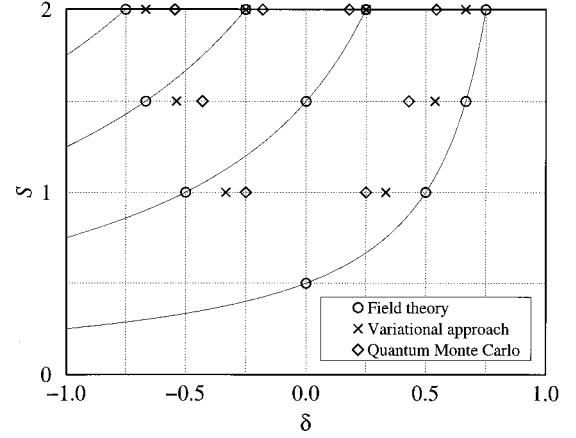


FIG. 8. Transition points in the spin Hamiltonian space spanned by the spin quantum number S and the alternating coupling δ , where the symbols \circ , \times , and \diamond denote the estimates obtained through the $O(3)$ nonlinear- σ -model quantum field theory, the variational approach, and the quantum Monte Carlo method, respectively. We also plotted the criterion for the critical behavior, $2S(1-\delta) = \pi \pmod{2\pi}$, which is predicted by the field-theoretical approach. The numerical uncertainty of the quantum Monte Carlo estimates is within the size of the symbols.

sality class as the $S=1/2$ Heisenberg model. In order to make sure of such a fascinating scenario, it is important to perform a further numerical specification of the critical points by means of various approaches. We hope that the present study will motivate further exploration into the topic.

ACKNOWLEDGMENTS

The author would like to express his special gratitude to S. Brehmer for fruitful discussion. It is also a pleasure to thank H.-J. Mikeska, H.-U. Everts, H. Tasaki, A. K. Kolezhuk, K. Totsuka, and M. Yamanaka for useful comments. The author is really grateful to Hannover Institute für Theoretische Physik for the hospitality during his stay there. Numerical calculations were mainly carried out on DEC Alpha stations at Osaka University and using the facilities of the Supercomputer Center, Institute for Solid State Physics, University of Tokyo. The present work was supported in part by Japanese Ministry of Education, Science, and Culture through a Grant-in-Aid (08740279), by German Ministry for Research and Technology under a contract (03MI4HAN8), and by a Grant-in-Aid from Ogasawara Foundation for the Promotion of Science & Engineering.

APPENDIX: CONCRETE FORMS OF THE g MATRICES

(a) $S=1, m=n=1$:

$$g_{2j-1}^A = g_{2j}^B = \begin{bmatrix} -|0\rangle & -\sqrt{2}|+1\rangle \\ \sqrt{2}|-1\rangle & |0\rangle \end{bmatrix}. \quad (A1)$$

(b) $S=1, m=2, n=0$:

$$g_{2j-1}^A = [|-1\rangle|0\rangle|+1\rangle], \quad (A2a)$$

$$g_{2j}^B = T[|+1\rangle|-1\rangle|0\rangle]. \quad (A2b)$$

(c) $S=3/2, m=2, n=1$:

$$g_{2j-1}^A = \begin{bmatrix} -|-\frac{1}{2}\rangle & -\sqrt{2}|+\frac{1}{2}\rangle & -\sqrt{3}|+\frac{3}{2}\rangle \\ \sqrt{3}|-\frac{3}{2}\rangle & \sqrt{2}|-\frac{1}{2}\rangle & |+\frac{1}{2}\rangle \end{bmatrix}, \quad (\text{A3a})$$

$$g_{2j}^B = T \begin{bmatrix} |+\frac{1}{2}\rangle & -\sqrt{2}|-\frac{1}{2}\rangle & \sqrt{3}|-\frac{3}{2}\rangle \\ \sqrt{3}|+\frac{3}{2}\rangle & -\sqrt{2}|+\frac{1}{2}\rangle & |-\frac{1}{2}\rangle \end{bmatrix}. \quad (\text{A3b})$$

(d) $S=3/2, m=3, n=0$:

$$g_{2j-1}^A = [|-\frac{3}{2}\rangle \quad |-\frac{1}{2}\rangle \quad |+\frac{1}{2}\rangle \quad |+\frac{3}{2}\rangle], \quad (\text{A4a})$$

$$g_{2j}^B = T [-|+\frac{3}{2}\rangle \quad |+\frac{1}{2}\rangle \quad -|-\frac{1}{2}\rangle \quad |-\frac{3}{2}\rangle]. \quad (\text{A4b})$$

(e) $S=2, m=n=2$:

$$g_{2j-1}^A = g_{2j}^B = \begin{bmatrix} |0\rangle & \sqrt{3}|+1\rangle & \sqrt{6}|+2\rangle \\ -\sqrt{3}|-1\rangle & -2|0\rangle & -\sqrt{3}|+1\rangle \\ \sqrt{6}|-2\rangle & \sqrt{3}|-1\rangle & |0\rangle \end{bmatrix}. \quad (\text{A5})$$

(f) $S=2, m=3, n=1$:

$$g_{2j-1}^A = \begin{bmatrix} -| -1\rangle & -\sqrt{2}|0\rangle & -\sqrt{3}|+1\rangle & -2|+2\rangle \\ 2| -2\rangle & \sqrt{3}| -1\rangle & \sqrt{2}|0\rangle & | +1\rangle \end{bmatrix}, \quad (\text{A6a})$$

$$g_{2j}^B = T \begin{bmatrix} -| +1\rangle & \sqrt{2}|0\rangle & -\sqrt{3}| -1\rangle & 2| -2\rangle \\ -2| +2\rangle & \sqrt{3}| +1\rangle & -\sqrt{2}|0\rangle & | -1\rangle \end{bmatrix}. \quad (\text{A6b})$$

(g) $S=2, m=4, n=0$:

$$g_{2j-1}^A = [| -2\rangle \quad | -1\rangle \quad |0\rangle \quad | +1\rangle \quad | +2\rangle], \quad (\text{A7a})$$

$$g_{2j}^B = T [| +2\rangle \quad -| +1\rangle \quad |0\rangle \quad -| -1\rangle \quad | -2\rangle]. \quad (\text{A7b})$$

Here, in comparison with the original definitions (2.4), some of the expressions have been adjusted with regard to their coefficients so as to simplify the actual calculations.

*Permanent address.

¹F. D. M. Haldane, Phys. Lett. **93A**, 464 (1983); Phys. Rev. Lett. **50**, 1153 (1983).

²R. Botet and R. Julien, Phys. Rev. B **27**, 613 (1983); R. Botet, R. Julien, and M. Kolb, *ibid.* **28**, 3914 (1983).

³S. Liang, Phys. Rev. Lett. **64**, 1597 (1990).

⁴S. R. White and D. A. Huse, Phys. Rev. B **48**, 3844 (1993).

⁵E. S. Sørensen and I. Affleck, Phys. Rev. Lett. **71**, 1633 (1993).

⁶O. Golinelli, Th. Jolicœur, and R. Lacaze, Phys. Rev. B **50**, 3037 (1994).

⁷N. Hatano and M. Suzuki, J. Phys. Soc. Jpn. **62**, 1346 (1993).

⁸S. V. Meshkov, Phys. Rev. B **48**, 6167 (1993).

⁹J. Deisz, M. Jarrell, and D. L. Cox, Phys. Rev. B **48**, 10227 (1993).

¹⁰Y. Nishiyama, K. Totsuka, N. Hatano, and M. Suzuki, J. Phys. Soc. Jpn. **64**, 414 (1995).

¹¹G. Sun, Phys. Rev. B **51**, 8370 (1995).

¹²U. Schollwöck and Th. Jolicœur, Europhys. Lett. **30**, 493 (1995).

¹³S. Yamamoto, Phys. Rev. Lett. **75**, 3348 (1995); **77**, 2845 (1996); U. Schollwöck and Th. Jolicœur, *ibid.* **77**, 2844 (1996).

¹⁴S. Yamamoto, Phys. Lett. A **213**, 102 (1996).

¹⁵S. Yamamoto, Phys. Rev. B **51**, 16 128 (1995).

¹⁶S. Yamamoto, Phys. Rev. B **52**, 10 170 (1995).

¹⁷K. Totsuka and M. Suzuki, J. Phys. Condens. Matter **7**, 1639 (1995).

¹⁸M. Yajima and M. Takahashi, J. Phys. Soc. Jpn. **65**, 39 (1996).

¹⁹M. Yamanaka, M. Oshikawa, and S. Miyashita, J. Phys. Soc. Jpn. **65**, 1562 (1996).

²⁰I. Affleck, Nucl. Phys. **B257**, 397 (1985); **B265**, 409 (1986).

²¹I. Affleck, in *Fields, Strings and Critical Phenomena*, Proceedings of the Les Houches School of Theoretical Physics, Session

XLIX, Haute-Savoie, 1988, edited by E. Brézin and J. Zinn-Justin (Elsevier, New York, 1989), p. 563.

²²R. R. P. Singh and M. P. Gelfand, Phys. Rev. Lett. **61**, 2133 (1988).

²³Y. Kato and A. Tanaka, J. Phys. Soc. Jpn. **63**, 1277 (1994).

²⁴S. Yamamoto, J. Phys. Soc. Jpn. **63**, 4327 (1994).

²⁵K. Totsuka, Y. Nishiyama, N. Hatano, and M. Suzuki, J. Phys. Condens. Matter **7**, 4895 (1995).

²⁶I. Affleck, T. Kennedy, E. H. Lieb, and H. Tasaki, Phys. Rev. Lett. **59**, 799 (1987); Commun. Math. Phys. **115**, 477 (1988).

²⁷M. Oshikawa, J. Phys. Condens. Matter **4**, 7469 (1992).

²⁸J. des Cloizeaux and J. J. Pearson, Phys. Rev. **128**, 2131 (1962).

²⁹H. J. Schulz, Phys. Rev. B **34**, 6372 (1986).

³⁰I. Affleck and F. D. M. Haldane, Phys. Rev. B **36**, 5291 (1987).

³¹A. Klümper, A. Schadschneider, and J. Zittartz, J. Phys. A **24**, L955 (1991); Z. Phys. B **87**, 281 (1992).

³²K. Totsuka and M. Suzuki, J. Phys. A **27**, 6443 (1994).

³³W.-D. Freitag and E. Müller-Hartmann, Z. Phys. B **83**, 381 (1991).

³⁴S. M. Girvin and D. P. Arovas, Phys. Scr. **T27**, 156 (1989).

³⁵S. Yamamoto and S. Miyashita, Phys. Rev. B **48**, 9528 (1993).

³⁶U. Schollwöck, Th. Jolicœur, and T. Garel, Phys. Rev. B **53**, 3304 (1996).

³⁷M. den Nijs and K. Rommelse, Phys. Rev. B **40**, 4709 (1989).

³⁸J. E. Hirsch, R. L. Sugar, D. J. Scalapino, and R. Blankenbecler, Phys. Rev. B **26**, 5033 (1982).

³⁹M. Suzuki, Prog. Theor. Phys. **56**, 1454 (1976).

⁴⁰S. Yamamoto, Phys. Rev. B **53**, 3364 (1996).

⁴¹T. Kennedy and H. Tasaki, Phys. Rev. B **45**, 304 (1992).

⁴²T. A. L. Ziman and H. J. Schulz, Phys. Rev. Lett. **59**, 140 (1987).

⁴³K. Hallberg, X. Q. G. Wang, P. Horsch, and A. Moreo, Phys. Rev. Lett. **76**, 4955 (1996).